This paper has been accepted for publication in *Chemistry – A European Journal* on 2017/11/15, and is published online with the DOI 10.1002/chem.201704651.

FULL PAPER

A valence-delocalised osmium dimer capable of dinitrogen photocleavage: ab initio insights into its electronic structure

V. Krewald*[a][b] and Leticia González*[a]

Abstract: The search for molecular catalysts that efficiently activate or cleave the dinitrogen molecule is an active field of research. While many thermal dinitrogen cleavage catalysts are known, the photochemical activation of N_2 has received considerably less attention. In this paper, we present the first computational study of the osmium dimer $[Os^{(II,III)}_2(\mu\text{-}N_2)(NH_3)_{10}]^{5+}$, which was shown to be capable of dinitrogen photocleavage. Despite its deceptively simple geometry, it has a complex electronic structure with a valence-delocalized and electronically degenerate ground state. Using multiconfigurational methods, we investigate the electronic structure at the ground state geometry and along the dinitrogen cleavage coordinate. Our results indicate that an unoccupied molecular orbital with σ-bonding character between osmium and μ-N atoms and σ-antibonding dinitrogen character is most affected by N-N distance elongation. This implies that a lower barrier for thermal or photochemical N_2 activation in linear M-N-N-M complexes can be achieved by lowering the energetic separation between this unoccupied orbital and the HOMO, representing a specific target for future catalyst design.

Introduction

The activation of dinitrogen is an important research target toward the development of sustainable routes to base chemicals that do not rely on fossil resources.[1] Industrially, the Haber–Bosch process converts dinitrogen into ammonia at a scale of hundreds of megatons per year, consuming approximately 1% of the world energy production.[2] Although it is an energy-efficient process,[3] it relies on dihydrogen usually taken from fossil resources and produces only NH_3 as the N-incorporating product.[2b] One route to a more sustainable Haber–Bosch process would be the use of dihydrogen and energy derived from renewable resources, e.g. from the oxidation of water;[4] however, such a process is not yet economically and industrially viable.[5]

Research in many synthetic, spectroscopic and computational laboratories is directed at better understanding Nature's dinitrogen-fixing FeMo complex and identifying homogeneous catalysts for dinitrogen activation.[6] The synthetic target for many molecular dinitrogen fixation catalysts is ammonia, usually formed via stepwise multiple additions of protons and electrons to a metal-bound and thus activated N_2.[6b, 7] An alternative is the dissociative dinitrogen reduction of a dimeric species into metal nitrido complexes, which is associated with a high kinetic barrier.[7e, 8] While one may at least question whether a molecular ammonia-producing catalyst will become economically competetive with the Haber–Bosch process in the near future, the large energy input required to reductively cleave N_2 to form metal nitrido species brings its own synthetic challenges. However, an advantage of metal nitrido complexes as synthetic intermediates is that they are amenable to a variety of further reactions to incorporate nitrogen atoms into base chemicals.[2b, 8a, 9] Ultimately, one could thus target molecules that are more valuable than NH_3, or devise synthetic routes that are more atom- and/or energy-efficient than using NH_3 derived from the Haber-Bosch process.

While many synthetic examples for transition metal complexes exist that fully or partially cleave the N_2 triple bond thermochemically, a photochemical route to activate dinitrogen is much less explored.[10] The photochemical activation of dinitrogen with solid-state catalysts was shown,[10b, 11] but only a small number of molecular catalysts are known that are capable of dinitrogen photocleavage upon irradiation with light from the UV or visible part of the spectrum.[9e, 12] All of these complexes contain a linear metal-nitrogen-nitrogen-metal unit with the metals molybdenum, osmium or tungsten. A single computational study on the photochemical activation of N_2 focused on similar complexes with ruthenium and iron cations.[13] In some of the experimental examples, the final product is a metal-nitrido complex, while in other cases the nitrogen atoms are incorporated into organic molecules. The electronic excitation and relaxation processes that lead to nitrogen-nitrogen bond cleavage, including a temporally resolved relaxation pathway, have been studied in detail only for a molybdenum dimer.[12c, 14]

Although the principle of photochemical dinitrogen activation has thus been demonstrated, the underlying mechanism is not understood and hence it is unclear how to systematically improve its efficiency. The most important obstruction appears to be the prevalence of undesired side reactions, for instance the cleavage of metal-nitrogen bonds and/or the relaxation to the dimer ground state without any bond cleavage.[12b, c] Regarding the driving force for dinitrogen photoactivation, a number of components are expected to play a role: absorption of several electronvolts of light energy, increase in entropy, and either formation of two metal-nitrido bonds instead of the strong dinitrogen bond or protonation of a species with diazene character.[13, 15]

A particularly interesting dinitrogen photocleavage complex is the mixed-valent Os(II)Os(III) complex $[Os^{(II,III)}_2(\mu\text{-}N_2)(NH_3)_{10}]^{5+}$, **1**, originally synthesized by Taube and coworkers (Fig. 1).[16] Upon irradiation of **1** with light at 3.40 eV or 4.88 eV, the complex cleaves into two metal-nitrido species, $[Os^{(V)}(N)(NH_3)_5]^{2+}$, $\mathbf{2}^{2+}$, and $[Os^{(VI)}(N)(NH_3)_5]^{3+}$, $\mathbf{2}^{3+}$, that undergo subsequent reactions to ultimately form two equivalents of $[Os^{(VI)}(N)(NH_3)_4]^{3+}$ (Fig. 1).[12b] It was also reported that the one-electron oxidized $Os(III)_2$ dimer does not undergo the dinitrogen cleavage reaction, but instead

[a] Dr V. Krewald, Prof. Dr L. González
Institute for Theoretical Chemistry, Faculty of Chemistry
University of Vienna
Währingerstr. 17, 1090 Vienna, Austria
E-mail: v.krewald@bath.ac.uk, leticia.gonzalez@univie.ac.at
[b] Dr V. Krewald
Department of Chemistry
University of Bath
Claverton Down, BA2 7AY, United Kingdom

Supporting information for this article is given via a link at the end of the document.

readily expels dinitrogen, i.e. cleaves the metal-nitrogen bond.[12b, 17]

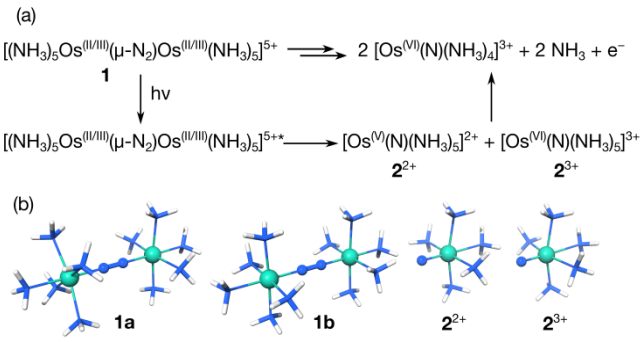

Figure 1. (a) Reaction sequence upon photochemical cleavage of complex **1**, $[Os^{(II,III)}_2(\mu\text{-}N_2)(NH_3)_{10}]^{5+}$, resulting first in the monomers $\mathbf{2}^{2+}$, $[Os^{(V)}(N)(NH_3)_5]^{2+}$, and $\mathbf{2}^{3+}$, $[Os^{(VI)}(N)(NH_3)_5]^{3+}$; (b) optimized geometries of **1a**, **1b**, $\mathbf{2}^{2+}$ and $\mathbf{2}^{3+}$.

This paper is the first to computationally characterize the electronic structure of the species involved in photochemical dinitrogen cleavage with the complex $[Os_2(\mu\text{-}N_2)(NH_3)_{10}]^{5+}$. Our main goal is to obtain fundamental insight into the electronic structure of complex **1** and the dinitrogen cleavage process with multiconfigurational electronic structure methods including spin-orbit coupling (SOC) effects. The calculated UV-vis absorption spectrum and the assignment of its features agrees well with the experiment. A scan along the N-N dissociation coordinate and the analysis of concomitant electronic structure changes yields valuable insights into the processes that need to occur during dinitrogen cleavage. It is found that the molecular orbital that undergoes most dramatic changes is of σ-bonding character between osmium and nitrogen atoms, and of σ-antibonding character between nitrogen atoms. We discuss the implications of our findings for the design of linear metal-nitrogen-nitrogen-metal complexes with improved thermal or photochemical dinitrogen activation efficiency.

Results and Discussion

Mixed-valent transition metal complexes such as **1** have been of interest to inorganic chemists for decades,[18] particularly because of their fascinating electronic structures. The most famous example is probably the Creutz-Taube ion, $[Ru_2(\mu\text{-py})(NH_3)_{10}]^{5+}$, which contains the same metal pentammine fragments as the osmium dimer studied here.[19] Robin and Day defined several categories for mixed-valent complexes depending on the localization or delocalization of the unpaired electrons, which were later refined to also include solvent effects and consider time scales for geometric changes of the complex and its solvent cage.[18c, 20] Briefly, the classes are as follows: (I) localized valences and no interaction between metal centers so that the complex has the properties of the isolated metal centers, (II) localized valences with a small barrier to electron transfer and a solvent cage that rearranges based on the current valence distribution, (III) delocalized valences, i.e. no barrier to electron transfer, in a solvent cage that accommodates the 'averaged' electronic and geometric structure, and (II-III) complexes with properties of classes II and III due to swiftly alternating localized valences in an averaged solvent cage. The Os_2(II,III) dimer investigated here is an example of a class III complex, as evidenced by its UV-vis absorption spectrum and the absence of nitrogen bridge vibrations in the IR spectrum.[12b, 21] During the dinitrogen bond cleavage process, a transition from the class III fully delocalized system to two class I fully localized systems, the osmium monomers, takes place.

Table 1. Interatomic distances [Å] and angles [°] for complexes **1a** and **1b** alongside literature reference values.

Distance [Å] or angle [°]	**1a**	**1b**	Lit.[a]	Lit.[b]
Os1-Os2	5.032	4.901	4.902	4.973
N1-N2	1.171	1.160	1.138	1.132
Os1-N1, Os2-N2	1.931, 1.930	1.870, 1.870	1.872, 1.893	1.968, 1.909
av. Os-N_{ax}	2.173	2.131	2.128	–
av. Os-N_{eq}	2.175	2.124	(2.013)	–
∠ Os-N-N	179.5, 179.8	179.8, 179.7	178.8, 179.6	171.5, 172.1

[a] $[(MeCN)(NH_3)_4Os(\mu\text{-}N_2)Os(NH_3)_4(MeCN)]^{5+}$; valence-delocalised; $\nu(N_2)$: –.[22] [b] *trans*,*trans*-$[(tpy)(Cl)_2Os^{III}(\mu\text{-}N_2)Os^{II}(Cl)_2(tpy)]^{+}$; valence-localised; $\nu(N_2)$: 2012 cm^{-1}.[24]

Complex **1** is not crystallographically characterized, and thus there was no alternative than to optimize the geometry with DFT, even though this is formally not a correct approach due to the degeneracy of its ground state**.** It will be seen later that the geometry obtained is indeed a minimum along the coordinate tested. Two equilibrium conformations were identified: one with a staggered arrangement of the ammonia groups when optimizing with a continuum solvation model for water (**1a**) and one with an eclipsed arrangement when optimizing in vacuum (**1b**). Although they differ in some key geometric parameters (Table 1), they possess near identical electronic structure properties (vide infra). Most importantly, the agreement of relevant structural parameters for **1a** and **1b** with related experimental data is excellent. Complex **1** is structurally similar to the valence-delocalised complex $[(MeCN)(NH_3)_4Os(\mu\text{-}N_2)Os(NH_3)_4(MeCN)]^{5+}$ in which acetonitrile groups instead of ammonia ligands coordinate *trans* to the η^1-η^1-dinitrogen bridge (Table 1).[22] The equatorial NH_3 ligands in the crystal structure of this complex are eclipsed, and thus the Os-Os, Os-N and N-N separations agree very closely with those of **1b**. The Os-Os and Os-N distances are longer in **1a**, but the N-N distance, a measure of the degree of N_2 activation, is only marginally longer (0.011 Å) than in **1b**.[23] It is also noted that there is a high degree of similarity between the two osmium

coordination environments in the crystal structure and the optimized geometries of **1a** and **1b**, which is taken as an indicator of valence delocalization. In contrast, the valence-localized *trans*,*trans*-[(tpy)(Cl)$_2$Os^{III}(μ-N$_2$)Os^{II}(Cl)$_2$(tpy)]$^+$ dimer features Os-N distances that differ by 0.059 Å as well as clearly bent Os-N-N angles (Table 1).

As a Robin-Day class (III) species, the unpaired electron in the *S* = 1/2 ground state of **1** is delocalized over both centers, and furthermore its ground state is electronically degenerate.[16, 25] To rationalize this behavior with molecular orbital (MO) theory, and to identify which orbitals should compose the active space in multiconfigurational calculations, the MO diagram for the linear Os-N-N-Os core with octahedrally coordinated osmium ions was constructed (Fig. 2). The MO nomenclature used throughout this paper indicates bonding and antibonding interactions between adjacent osmium and nitrogen atoms in the linear Os-N-N-Os core; for example, a π-π*-π orbital is bonding between nitrogen and osmium atoms and antibonding between nitrogen atoms.

The two π*-π-π* orbitals carry three electrons in the ground state, correctly representing its degeneracy. The two lower π-type orbitals are fully occupied whereas the all-antibonding π*-π*-π* orbital is unoccupied. Of the four sets of σ-type interactions between the osmium d(z^2) and nitrogen p(z) orbitals, only the lowest one is occupied. Finally, the lower set of δ/δ* orbitals based on the d(xy) orbitals is fully occupied whereas the higher set formed by the d(x^2-y^2) orbitals is empty. The MO diagram is consistent with the partial MO diagram derived from an effective Hamiltonian by Dubicki et al.[26]

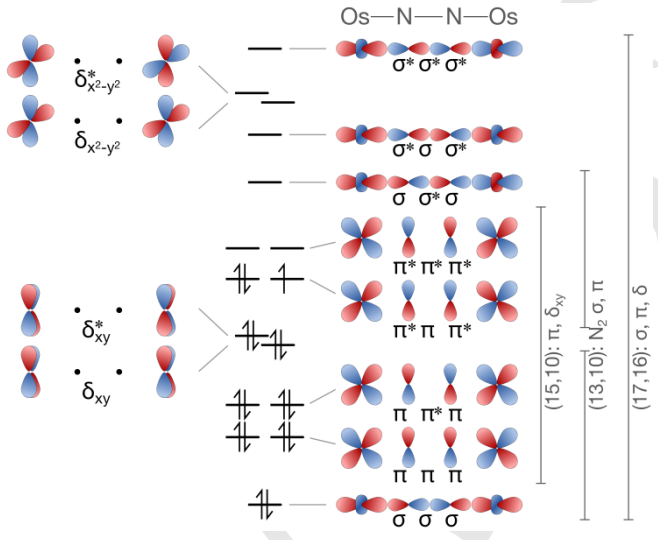

Figure 2. Molecular orbital scheme and sketches of the molecular orbitals for **1**$^{5+}$, [Os$^{(II,III)}$$_2$(μ-N$_2$)(NH$_3$)$_{10}$]$^{5+}$; energetic spacings are not to scale. Bars on the right indicate the orbitals included in the active spaces (15,10), (13,10) and (17,16). See main text for label nomenclature.

Given the degenerate ground state of this complex, multiconfigurational complete active space self consistent field (CASSCF) and its second-order perturbation theory-corrected (CASPT2) variant are the most appropriate methods to quantitatively evaluate its electronic structure and excited states. A full-valence active space including ten metal d-orbitals and six nitrogen p-orbitals would be represented as a (17,16) active space in the (electrons, orbitals) nomenclature commonly used. In all electronic states of **1**, many individual configurations of the same character, e.g. π*-π-π*→π*-π*-π* excitations, contribute to the wavefunction. While their individual weights are quite small, they accumulate significant weights when summed up, so that we will use such 'combined weights', in the following to quantitate their total contribution (Table 2).

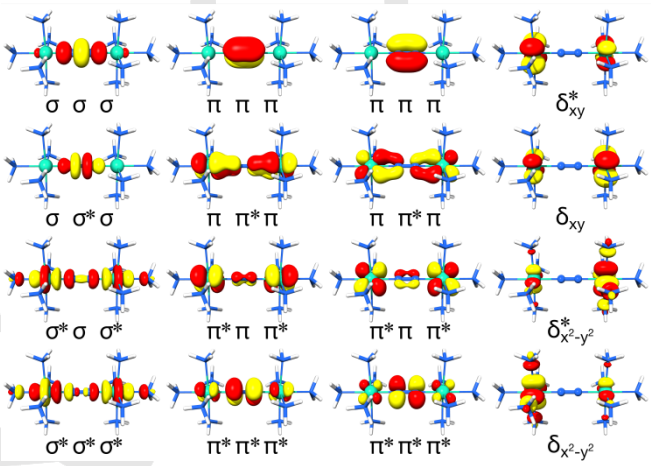

Figure 3. Orbitals obtained for **1b** from a CASSCF (17,16) calculation of six states with the ANO-RCC-MB basis set. Orbital labels are the same as in Figure 1. Color code of the atoms is Os: green, N: blue, H: grey.

A CASSCF (17,16) calculation on **1b** resulted in molecular orbitals similar in character to those expected from MO theory (Fig. 3). Table 2 lists the CASSCF coefficients (c^2_{CAS}) of all states discussed in the following along with the spin-orbit-coupled CASPT2 (SO-CASPT2, vide infra) energies; CASSCF and CASPT2 energies are shown in the SI (Table S1). The two lowest doublet states are separated by 0.07 eV. The electronic structure of these two states (E_1) that compose the degenerate ground state corresponds essentially to the configuration shown in Fig. 2, $(σ\text{-}σ\text{-}σ)^2(π\text{-}π\text{-}π)^4(π\text{-}π^*\text{-}π)^4(δ_{xy})^2(δ^*_{xy})^2(π^*\text{-}π\text{-}π^*)^3(π^*\text{-}π^*\text{-}π^*)^0(σ\text{-}σ^*\text{-}σ)^0(σ^*\text{-}σ\text{-}σ^*)^0(δ_{x2\text{-}y2})^0(δ^*_{x2\text{-}y2})^0(σ^*\text{-}σ^*\text{-}σ^*)^0$ (c^2_{CAS}: 0.760/0.758, Table 2), with a small contribution from a configuration where an electron from a π*-π-π* orbital is excited to a π*-π*-π* orbital (c^2_{CAS}: 0.105/0.105). The excited states appear as pairs of excitations. The lowest pair of excited states (E_2) at ca. 0.6 eV is dominated by excitations from the $δ_{xy}/δ^*_{xy}$ level to the π*-π-π* SOMO (c^2_{CAS}: 0.690/0.690), with a minor contribution of an excitation from the same orbital into the π*-π*-π* orbitals (c^2_{CAS}: 0.155/0.155). The two highest states (E_3) calculated are due to excitations from the π-π*-π orbitals into the π*-π-π* SOMO (c^2_{CAS}: 0.590/0.592) with a small component due to excitations from the HOMOs into orbitals of π*-π*-π* character (c^2_{CAS}: 0.219/0.221).

Based on these CASSCF results, the degree of N_2 activation in **1** can be quantitated by calculating the effective bond order

(EBO)[27] according to EBO = (η_b– η_{ab})/2, in which η_b is the sum of occupation numbers for the bonding orbitals and η_{ab} that for the antibonding orbitals. Taking the σ-σ-σ, π-π-π, π*-π-π* and σ*-σ-σ* orbitals as N-N bonding and the π-π*-π, π*-π*-π*, σ-σ*-σ and σ*-σ*-σ* as N-N antibonding, the EBO calculated from their occupation numbers is 2.37, indicative of a small degree of N-N bond activation and in agreement with expectations.[12b, 16]

Figure 4 shows the experimental UV-vis absorption spectrum of $\mathbf{1}^{5+}$, which contains five distinct features below 2 eV (Fig. 5; blue traces digitized from Refs. [26] and [12b]). Based on an effective Hamiltonian for the dimer and considering which bands would be dipole-allowed or vibronically induced, Dubicki et al.[26] assigned these bands as follows: the lowest energy absorption as a vibrationally induced state due to SOC of the Os(d^5) configuration; the two close-lying bands at ca. 0.6 eV as transitions involving the $\delta_{xy}/\delta^*_{xy}$ level; the low-intensity transition at ca. 1.1 eV as parity-forbidden transition from orbitals of $\delta_{xy}/\delta^*_{xy}$ and π character; and the intense and asymmetric band at 1.7–2.0 eV as due to a transition from orbitals of $\delta_{xy}/\delta^*_{xy}$ and π character for the lower-energy component and orbitals of π character for the higher-energy component.

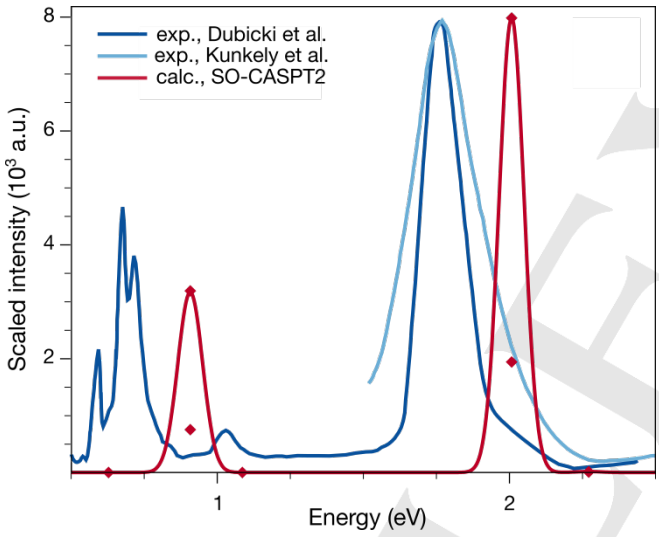

Figure 4. UV-vis absorption spectrum of **1** (digitized from [26] (dark blue) and [12b] (light blue)) and predicted UV-vis spectra based on spin-orbit coupled CASPT2(17,16) with ANO-RCC-MB basis set; calculated intensities (red diamonds) are scaled to the most intense transition at 8000 a.u.; the convoluted spectrum is broadened with Gaussian lineshapes (0.1 eV FWHM).

To calculate the UV-vis spectrum, the twelve spin-orbit coupled states resulting from the six CASPT2 (17,16) roots were used (Fig. 4, red trace). The CASPT2 (17,16) calculations show large and consistent reference weights of 0.7336-0.7344, and while the relative energies of the four lowest states are only slightly modified, the two highest states the energy increases by 0.11 eV and 0.12 eV (details in Table S1). Spin-orbit coupling of each degenerate doublet state (E_i) leads to four states (D_n', D_n'', D_{n+1}', D_{n+1}''). The dominant spin-orbit interactions between the six CASPT2 states leading to twelve SO-CASPT2 states are illustrated in Figure 5; their SOC coefficients (c^2_{SOC}) are listed in Table 2. Quartet states are found much higher in energy (> 3eV above the ground state, vide infra) and therefore are not considered here.

The electronic transitions between the D_1'/D_1'' and D_2'/D_2'' set of states are predicted at 0.63 eV (Table 2). At 0.91 eV, transitions of the type δ(xy)/δ(xy)*→π*-π-π* with small admixtures of π-π*-π→π*-π-π* are found ($D_1'→D_3'/D_1''→D_3''$ and $D_1'→D_3''/D_1''→D_3'$). These transitions carry significant intensity (Fig. 4, Table 2). The transitions predicted at 1.09 eV ($D_1'→D_4'/D_1''→D_4'$ and $D_1'→D_4''/D_1''→D_4'$) stem from the same CASSCF roots, but differ in their SOC mixing coefficients. At 2.01 eV and 2.27 eV, transitions to spin-orbit coupled states of π-π*-π→π*-π-π* with admixture of π*-π-π*→π*-π*-π* character are found ($D_1'→D_5'/D_1''→D_5'$ and $D_1'→D_5''/D_1''→D_5'$; $D_1'→D_6'/D_1''→D_6'$ and $D_1'→D_6''/D_1''→D_6'$). The lower-energy transition of this set is predicted as the most intense in the spectral range considererd.

The overall agreement of the predicted bands and their intensities with the experimental spectrum is quite satisfactory: the parity-allowed and thus intense transitions are predicted correctly, albeit blue-shifted, while the parity-forbidden transitions do not carry significant intensity since no vibrational effects are considered. It is noted that the splitting of the second-lowest experimental feature is not reproduced by our gas-phase calculations.

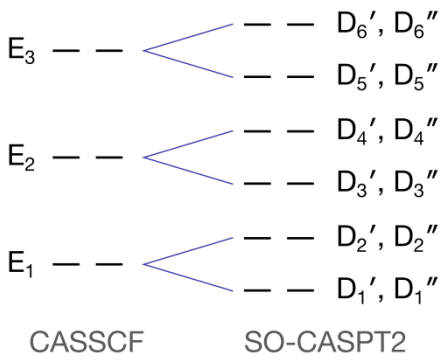

Figure 5. Schematic depiction of the CASSCF energy levels of the six lowest states (two degenerate states in each E_n state), and the states resulting from SO-CASPT (two degenerate states D_n', D_n'' in each set).

While the (17,16) active space CASPT2/CASSCF calculations are feasible for selected single points, they are prohibitively expensive to use in a reaction coordinate scan. It is therefore desirable to identify smaller active spaces that would describe the electronic structure with sufficient accuracy. Rationales for not including specific orbitals in the active space are their energetic separation from the HOMO-LUMO gap or their MO symmetry. This approach of not including all metal valence d orbitals in the active space has been employed successfully by several groups and for different types of problem, including metal-metal bonding, magnetic couplings and redox potentials.[27c, 28]

For **1**, two smaller active spaces than the full-valence (17,16) active space render useful insights: a (15,10) active space that includes all molecular orbitals of π-symmetry and the

energetically lower set of δ/δ* orbitals, and a (13,10) active space that includes all π-type MOs as well as the energetically lowest σ-type MOs that are dominated by N p(z) character (see Fig. 2). With the smaller active spaces, calculations with a larger basis set on osmium ions and nitrogen ligands were feasible (ANO-RCC-VDZP instead of ANO-RCC-MB); however basis set effects are found to be small (Table S2). Moreover, the electronic structure differences for the two geometric conformations are also small (Table S3), indicating that **1** is dominated by the σ- and π-interactions of the linear Os-N-N-Os core. The validity of these electronic structure representations is confirmed by comparing the state character and electronic excitation energies against the larger (17,16) active space.

Table 2. Spin-coupled CASPT2 energies (eV), oscillator strenghts f (•10^3), spin-orbit coupling coefficients ($c^2_{SOC} > 0.10$), CASSCF coefficients (c^2_{CAS}) and character of most significant contributing configurations for **1b**(17,16) and **1a**(15,10) based on the six lowest CASSCF states E_n, and **1a**(13,10) based on the four lowest CASSCF states E_n. The ground state is degenerate (D_1', D_1''), see Figure 5 for the relationship between the E_n and D_n components. The degenerate excitations $D_1' \rightarrow D_n'$ / $D_1'' \rightarrow D_n''$ and $D_1' \rightarrow D_n''$ / $D_1'' \rightarrow D_n'$ differ only in their oscillator strength ($f(D_1' \rightarrow D_n') = f(D_1'' \rightarrow D_n'') \neq f(D_1' \rightarrow D_n'') = f(D_1'' \rightarrow D_n')$); only those originating from D_1' are shown.

	1b(17,16)				**1a**(15,10)				**1a**(13,10)				
	ΔE	f	c^2_{SOC}	c^2_{CAS}	ΔE	f	c^2_{SOC}	c^2_{CAS}	ΔE	f	c^2_{SOC}	c^2_{CAS}	Character of E_n configurations
D_1', D_1''	0.000	–	0.500	0.760 0.105	0.000	–	0.472	0.614 0.301	0.000	–	0.547	0.687 0.205	$(\pi^*\text{-}\pi\text{-}\pi^*)^3$ $(\pi\text{-}\pi^*\text{-}\pi)^3$ $(\pi^*\text{-}\pi\text{-}\pi^*)^3$ $(\pi^*\text{-}\pi^*\text{-}\pi^*)^1$
			0.393	0.758 0.105			0.405	0.614 0.296			0.453	0.687 0.202	$(\pi^*\text{-}\pi\text{-}\pi^*)^3$ $(\pi\text{-}\pi^*\text{-}\pi)^3$ $(\pi^*\text{-}\pi\text{-}\pi^*)^3$ $(\pi^*\text{-}\pi^*\text{-}\pi^*)^1$
D_2'; D_2''	0.627	0.001; 0.000	0.550	0.758 0.105	0.579	0.002; 0.001	0.527	0.614 0.296	0.463	0.000; 0.001	0.547	0.687 0.202	$(\pi^*\text{-}\pi\text{-}\pi^*)^3$ $(\pi\text{-}\pi^*\text{-}\pi)^3$ $(\pi^*\text{-}\pi\text{-}\pi^*)^3$ $(\pi^*\text{-}\pi^*\text{-}\pi^*)^1$
			0.449	0.760 0.105			0.470	0.614 0.301			0.453	0.687 0.205	$(\pi^*\text{-}\pi\text{-}\pi^*)^3$ $(\pi\text{-}\pi^*\text{-}\pi)^3$ $(\pi^*\text{-}\pi\text{-}\pi^*)^3$ $(\pi^*\text{-}\pi^*\text{-}\pi^*)^1$
D_3'; D_3''	0.907	4.896; 1.154	0.719	0.690 0.155	0.791	1.057; 3.075	0.489	0.579 0.207	–	–	–	–	$(\delta/\delta^*(xy))^3$ $(\pi^*\text{-}\pi\text{-}\pi^*)^4$ $(\delta/\delta^*(xy))^3$ $(\pi^*\text{-}\pi\text{-}\pi^*)^3$ $(\pi^*\text{-}\pi^*\text{-}\pi^*)^1$
			0.223	0.690 0.155			0.442	0.578 0.208					$(\delta/\delta^*(xy))^3$ $(\pi^*\text{-}\pi\text{-}\pi^*)^4$ $(\delta/\delta^*(xy))^3$ $(\pi^*\text{-}\pi\text{-}\pi^*)^3$ $(\pi^*\text{-}\pi^*\text{-}\pi^*)^1$
D_4'; D_4''	1.085	0.000; 0.000	0.681	0.690 0.155	0.972	0.003; 0.003	0.462	0.578 0.208	–	–	–	–	$(\delta/\delta^*(xy))^3$ $(\pi^*\text{-}\pi\text{-}\pi^*)^4$ $(\delta/\delta^*(xy))^3$ $(\pi^*\text{-}\pi\text{-}\pi^*)^3$ $(\pi^*\text{-}\pi^*\text{-}\pi^*)^1$
			0.211	0.690 0.155			0.414	0.579 0.207					$(\delta/\delta^*(xy))^3$ $(\pi^*\text{-}\pi\text{-}\pi^*)^4$ $(\delta/\delta^*(xy))^3$ $(\pi^*\text{-}\pi\text{-}\pi^*)^3$ $(\pi^*\text{-}\pi^*\text{-}\pi^*)^1$
D_5'; D_5''	2.008	2.980; 12.254	0.569	0.590 0.219	1.757	1.869; 5.419	0.491	0.436 0.272	1.573	3.581; 13.745	0.525	0.533 0.252	$(\pi\text{-}\pi^*\text{-}\pi)^1$ $(\pi^*\text{-}\pi\text{-}\pi^*)^4$ $(\pi^*\text{-}\pi\text{-}\pi^*)^2$ $(\pi^*\text{-}\pi^*\text{-}\pi^*)^1$
			0.373	0.592 0.221			0.438	0.439 0.270			0.473	0.535 0.250	$(\pi\text{-}\pi^*\text{-}\pi)^1$ $(\pi^*\text{-}\pi\text{-}\pi^*)^4$ $(\pi^*\text{-}\pi\text{-}\pi^*)^2$ $(\pi^*\text{-}\pi^*\text{-}\pi^*)^1$
D_6; D_6'	2.272	0.010; 0.022	0.600	0.592 0.221	1.981	0.008; 0.002	0.525	0.439 0.270	1.867	0.001; 0.000	0.525	0.535 0.250	$(\pi\text{-}\pi^*\text{-}\pi)^1$ $(\pi^*\text{-}\pi\text{-}\pi^*)^4$ $(\pi^*\text{-}\pi\text{-}\pi^*)^2$ $(\pi^*\text{-}\pi^*\text{-}\pi^*)^1$
			0.400	0.590 0.219			0.471	0.436 0.272			0.473	0.533 0.252	$(\pi\text{-}\pi^*\text{-}\pi)^1$ $(\pi^*\text{-}\pi\text{-}\pi^*)^4$ $(\pi^*\text{-}\pi\text{-}\pi^*)^2$ $(\pi^*\text{-}\pi^*\text{-}\pi^*)^1$

To achieve a balanced excitation level spectrum for **1a** with CASSCF(15,10) that extends into the regions of interest for photocleavage excitations (E_{exp}: 3.40 eV, 4.88 eV), 38 states had to be calculated. While the six lowest CASSCF states are well separated at ca. 0.0 eV, 0.5 eV, and 1.4 eV, the following 7-36 states span from 3.2-3.8 eV, above which states 37 and 38 are found at 6.6 eV. If a larger number of states was calculated, the next two states would follow at ca. 7.3 eV. Instead of discussing the character all these different excitations in detail, a broad overview of their compositions is given next, while more details

on state energies, CASPT2 weights and occupation numbers are provided in the SI (Table S4).

The two lowest CASSCF (15,10) roots represent the degenerate ground state at 0.00/0.04 eV, for which the dominant configurations (c^2_{CAS}: 0.614/0.614) and the minor configurations (c^2_{CAS}: 0.301/0.296) correspond to that found for the (17,16) active space (Table 2). Similarly for the following two CASSCF roots, the excitation character can be clearly assigned as dominantly δ(xy)/δ(xy)* → π*-π-π* (c^2_{CAS}: 0.579/0.578), with a smaller component of δ(xy)/δ(xy)* → π*-π*-π* (c^2_{CAS}: 0.207/0.208). At higher energies, excitations between orbitals of π character dominate: the major configurations are of π-π*-π → π*-π-π* character (c^2_{CAS}: 0.436/0.439), while a second type of excitation, π*-π-π*→π*-π*-π*, accumulates weights of 0.272/0.270 over five individual configurations.

The dense set of states between 3.2-3.8 eV extends beyond those predicted for the (17,16) active space. These excitations fall into two categories: those from δ(xy)/δ(xy)* orbitals into orbitals of π character (9, 10, 13-20, 22, 23, 27-32), and excitations between orbitals of π character (11, 21, 24-26, 33-36). While in the lowest six roots, the combined weight of double (and in rare cases higher) excitations already accumulate up to 0.190 over up to 13 individual configurations, for states 7 and above double (and higher) excitations can be the dominant with combined weights of around 0.5 or higher. Most notable in this respect are states 19 and 20, where two configurations with individual weights of 0.915 and 0.918 represent a double excitation of one electron from each δ(xy)/δ(xy)* orbital into one π*-π-π* and one π*-π*-π* orbital. The highest states calculated at 6.61 eV and 6.62 eV are dominated by π-π-π → π*-π-π* excitations, but with up to 39 individual configurations they are not as well defined as the lower states.

The effects of dynamic correlation for the CASSCF(15,10) description were explored with CASPT2 calculations. For all states of well-defined character (i.e. all expect the highest two doublet states), CASPT2 modifies the energy as expected (see Table S4). The SO-CASPT2(15,10) calculation yields D_n'/D_n'' states of very similar spin state admixture and energies as for the CASSCF(17,16) calculation. The three lowest resulting excited states are within 0.2 eV of the SO-CASPT2(17,16) states, while the energetic difference with the two highest states are larger (0.25 eV, 0.29 eV). A CASPT2(15,10) calculation with 18 quartet roots showed that these fall in the same energetic region (3.61-4.52 eV) as the dense set of doublet states (details in Table S4).

To cleave the N-N bond, an orbital of N-N σ* character must become occupied. An active space that includes the N(p_z)-dominated σ-σ-σ and σ-σ*-σ orbitals as well as the π-π-π, π-π*-π, π*-π-π* and π*-π*-π* orbitals conforms to a CASSCF(13,10). The 18 states calculated with this active space extend up to 6.8 eV. Fortunately, the CASSCF (13,10) E_1 ground state is of identical character to that in the (17,16) and (15,10) calculations (see Table 2). As no orbitals of δ(xy)/δ(xy)* character are included in this active space, no states corresponding to the E_2 type in the (17,16) and (15,10) active spaces can be predicted, and no SO-CASPT2 states of D_3'/D_3'' and D_4'/D_4'' character are found. The following two states of E_3 character are dominated by π-π*-π→ π*-π-π* (c^2_{CAS}: 0.533/0.535) and π*-π-π* → π*-π*-π*, (c^2_{CAS}: 0.252/0.250), exactly as for the CASSCF (17,16) and CASSCF (15,10) active spaces. Twelve CASSCF states fall between 3.30 eV and 3.89 eV which are dominated by excitations of π*-π-π*→ π*-π*-π* and π-π*-π → π*-π*-π* character (Table S5). Their character corresponds exactly to the states of similar character found for the (15,10) active space. At 6.82 eV, two excitations of π-π-π→π*-π-π* character are found. Similar to the (15,10) active space, a dense set of eight quartet states are found between 3.64 eV and 4.53 eV with CASPT2, with four further higher-energy quartet states around 7 eV. The agreement of the four lowest SO-CASPT2(13,10) states with those of the larger active spaces is excellent both in terms of state character and relative energies (differences < 0.2 eV). The discrepancies in relative energies for the two highest states are slightly larger (0.44 eV, 0.41 eV for (13,10)). Most importantly, however, the energetic order of the states and the state character does not change.

The above results show that for **1**, smaller active spaces are a reliable approximation of the full valence active space at greatly reduced computational cost. This permits the distortion of the osmium dimer along relevant reaction coordinates. Ultimately, two separated osmium dimers will result, a closed-shell $[Os^{(VI)}(N)(NH_3)_5]^{3+}$ and an open-shell $[Os^{(V)}(N)(NH_3)_5]^{2+}$ that carries the excess electron until the subsequent reactions shown in Fig. 1 have taken place. The electronic structure of these two monomers was characterized with the same SO-CASPT2/CASSCF approach as for the dimer. Monomer $\mathbf{2}^{3+}$ has the expected single-configurational characer with high-lying electronic excitations (> 4 eV). Including the N 2s orbital and the bonding orbital of the d(x^2-y^2) with the equatorial ligands has little effect on the predicted state energies (Table S6). For $\mathbf{2}^{2+}$, a degenerate ground state best described as $(\sigma)^2(\pi)^4(d_{xy})^2(\pi^*)^1(d_{x2\text{-}y2})^0(\sigma^*)^0$ and low-lying electronically excited states at ca. 0.3 eV and 1.7 eV are found (Table S6).

The N_2 cleavage process can be considered complete once the orbital dominated by the N-N σ* interaction is doubly occupied, as this corresponds to the expected electronic configuration for two separated monomers. Even though 40 CASSCF states extending to 9.8 eV were calculated with the (13,10) active space at the ground state geometry of **1**, the σ-σ*-σ orbital was not significantly occupied in any of them (occupation number <0.020). To understand how the electronic structure is affected upon elongation of the N-N distance, a CASSCF scan along this coordinate with the (13,10) active space and its twelve lowest doublet roots was performed. The geometries were constructed manually by increasing the N-N distance and keeping the remainder of the geometry frozen (Figure 6). Other dissociation pathways are discussed in the literature, including those with a so-called 'zig-zag' species containing a diazene moijety that has a N-N bridge double bond and lone pairs at the nitrogen atoms,[13, 29] however as a first exploration of the dissociation of **1**, which is known to yield metal nitrido complexes, the linear reaction coordinate appears most relevant.

Figure 6(a) shows that upon elongating the N-N distance, the two degenerate CASSCF $(\pi^*\text{-}\pi\text{-}\pi^*)^1$ ground states (dark blue) increase significantly in total energy but remain lowest up to a separation of 1.87 Å. Beyond that, four states (green; E_7, E_8, E_9, E_{10}) with very similar energies that are all dominated by configurations with a singly occupied σ-σ*-σ orbital are lowest in energy. At an N-N separation of 2.47 Å, two states (red; E_{12}, E_{13}) with $(\sigma\text{-}\sigma\text{-}\sigma)^2(\pi\text{-}\pi\text{-}\pi)^4(\pi\text{-}\pi^*\text{-}\pi)^4(\pi^*\text{-}\pi\text{-}\pi^*)^1(\pi^*\text{-}\pi^*\text{-}\pi^*)^0(\sigma\text{-}\sigma^*\text{-}\sigma)^2$ configurations are lowest in energy—exactly as it would be expected for a distorted structure with monomer character in the fragments. The CASSCF weights of these configurations are larger than 0.58 at 2.47 Å N-N separation, comparable to the

weight of the dominant ground state configuration at the equilibrium geometry. A second set of two states (orange; E_{17}, E_{18}) with $(\sigma\text{-}\sigma\text{-}\sigma)^2(\pi\text{-}\pi\text{-}\pi)^4(\pi\text{-}\pi^*\text{-}\pi)^4(\pi^*\text{-}\pi\text{-}\pi^*)^0(\pi^*\text{-}\pi^*\text{-}\pi^*)^1(\sigma\text{-}\sigma^*\text{-}\sigma)^2$ configurations also lowers significantly in energy at an N-N distance of 2.47 Å. These states are expected to become degenerate with the ground state at even longer distances as the π*-π-π* and π*-π*-π* MOs transition into the four monomeric Os-N π* MOs (vide infra). However, since the (13,10) active space does not include the osmium d(z^2) orbitals, the scan cannot be completed to fully independent monomers.

We note that in a relaxed scan, the Os-N bond length would contract significantly upon depopulation of the π*-π-π* orbitals, but this is not expected to qualitatively change the state ordering and changes in ground state character along the N-N dissociation coordinate. The geometric effect of a partially occupied Os-N π* orbital is exemplified in the Os-N bond lengths of the two monomer products, where the Os(V)-N bond in $\mathbf{2}^{2+}$ is 0.089 Å longer than the Os(VI)-N bond in $\mathbf{2}^{3+}$.

To obtain a picture that includes SOC effects, the CASSCF states at each point of the scan were used to obtain SO-CASPT2 doublet states (Table 3, Figure 6b). While up to an N-N separation of 1.47 Å, only the doublet states within an E_n set couple, SOC induces mixing between states of different character at larger separations, e.g. at the crossing of the E_2 and E_3 states at ca. 1.57 Å. At 1.87 Å N-N distance, the new states E_7, E_8, E_9, and E_{10}, which are dominated by configrations with a singly occupied σ-σ*-σ orbital, contribute significantly to the SO-CASPT2 states 3 and 4. The final ground state configurations E_{12} and E_{13} first contribute to the SO-CASPT2 states 6-9 at 2.07 Å N-N separation and dominate the two lowest states from a dinitrogen distance of 2.47 Å onwards. The overall interpretation of the dinitrogen dissociation process is not altered upon consideration of SOC effects.

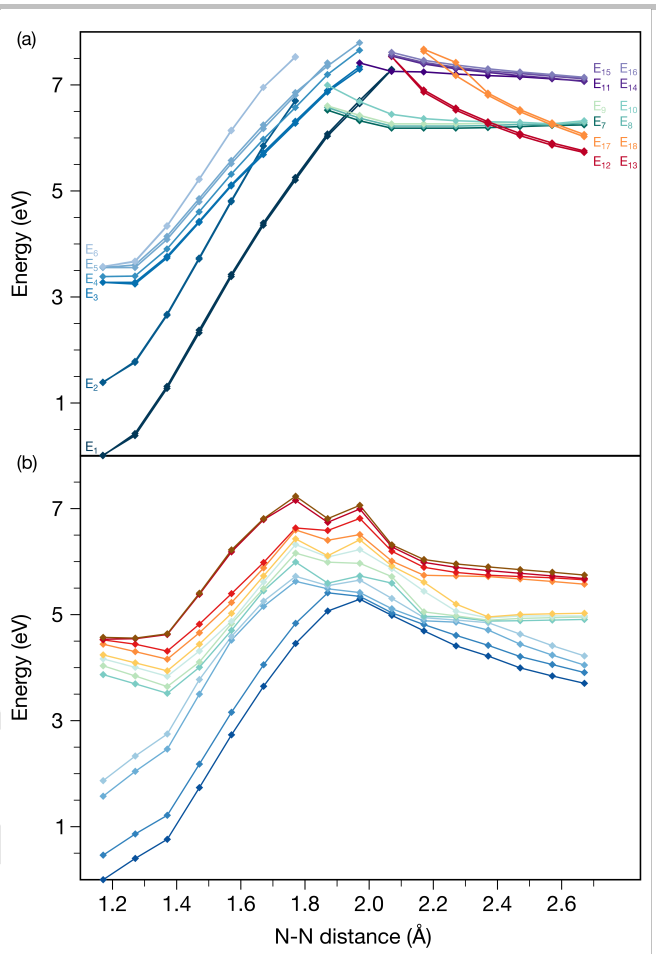

Figure 6. Electronic structure changes upon elongation of the N-N distance in **1** obtained by SO-CASPT2/CASSCF calculations. (a) 12 lowest CASSCF(13,10) states along the N-N separation coordinate. (b) SO-CASPT2 doublet states obtained with the 12 states in (a), resulting in 24 pairwise degenerate states colored blue to brown at each point of the scan in order of increasing energy (see Table 3 for composition).

Table 3. SO-CASPT2 energies (eV) and state compositions in terms of spin-orbit coupling coefficients (c^2_{SOC} > 0.15) and identity of CASSCF configurations for 13 of the 16 steps of the N-N scan (full data in Table S8). Of the 24 SO-CASPT2 states obtained from 12 CASSCF states only one of the pairwise degenerate states (D_n', D_n'') is shown. Where applicable, degenerate components of the CASSCF E_n states are differentiated as E_n, $E_n^{\cdot}$. Final ground state components in bold.

d_{NN}/Å	1	2	3	4	5	6	7	8	9	10	11	12
	1.74	2.18	3.50	3.78	4.01	4.11	4.31	4.44	4.66	4.82	5.38	5.40
1.47	0.55 $E_1^{\cdot}$ 0.45 E_1	0.55 E_1 0.45 $E_1^{\cdot}$	0.53 $E_2^{\cdot}$ 0.46 E_2	0.52 E_2 0.45 $E_2^{\cdot}$	0.60 $E_3^{\cdot}$ 0.30 E_3	0.63 E_3 0.31 $E_3^{\cdot}$	0.51 E_4 0.48 $E_4^{\cdot}$	0.51 $E_4^{\cdot}$ 0.48 E_4	0.67 $E_5^{\cdot}$ 0.26 E_5	0.69 $E_5^{\cdot}$ 0.26 E_5	0.78 $E_6^{\cdot}$ 0.22 E_6	0.78 E_6 0.22 $E_6^{\cdot}$
	2.73	3.16	4.52	4.59	4.70	4.83	4.87	5.02	5.23	5.40	6.18	6.22
1.57	0.55 $E_1^{\cdot}$ 0.45 E_1	0.55 E_1 0.45 $E_1^{\cdot}$	0.40 E_2 0.34 E_3	0.49 $E_2^{\cdot}$ 0.36 $E_3^{\cdot}$	0.45 $E_3^{\cdot}$ 0.26 $E_2^{\cdot}$	0.50 E_3 0.40 E_2	0.51 E_4 0.48 $E_4^{\cdot}$	0.51 $E_4^{\cdot}$ 0.48 E_4	0.66 $E_5^{\cdot}$ 0.26 E_5	0.68 $E_5^{\cdot}$ 0.27 E_5	0.66 $E_6^{\cdot}$ 0.34 E_6	0.66 E_6 0.34 $E_6^{\cdot}$
	3.65	4.05	5.16	5.25	5.45	5.49	5.62	5.73	5.88	5.98	6.79	6.81
1.67	0.55 $E_1^{\cdot}$ 0.45 E_1	0.55 E_1 0.45 $E_1^{\cdot}$	0.64 $E_3^{\cdot}$ 0.31 E_3	0.65 E_3 0.32 $E_3^{\cdot}$	0.51 $E_2^{\cdot}$ 0.49 E_2	0.50 E_4 0.45 $E_4^{\cdot}$	0.51 E_2 0.48 $E_2^{\cdot}$	0.37 $E_4^{\cdot}$ 0.23 E_4 0.22 $E_2^{\cdot}$	0.34 E_2 0.30 $E_4^{\cdot}$ 0.29 E_4	0.66 $E_5^{\cdot}$ 0.27 E_5	0.53 $E_6^{\cdot}$ 0.47 E_6	0.53 E_6 0.47 $E_6^{\cdot}$
	4.46	4.84	5.63	5.72	5.99	6.16	6.32	6.43	6.60	6.64	7.15	7.23
1.77	0.55 $E_1^{\cdot}$ 0.44 E_1	0.55 E_1 0.44 $E_1^{\cdot}$	0.68 $E_3^{\cdot}$ 0.29 E_3	0.67 E_3 0.29 $E_3^{\cdot}$	0.51 $E_4^{\cdot}$ 0.48 E_4	0.50 E_4 0.46 $E_4^{\cdot}$	0.47 E_2 0.43 $E_2^{\cdot}$	0.52 $E_5^{\cdot}$ 0.41 E_5	0.44 $E_5^{\cdot}$ 0.41 E_5	0.51 $E_2^{\cdot}$ 0.37 E_2	0.61 $E_6^{\cdot}$ 0.39 E_6	0.61 E_6 0.39 $E_6^{\cdot}$
	5.07	5.41	5.49	5.55	5.59	5.99	6.09	6.11	6.40	6.59	6.74	6.81
1.87	0.55 $E_1^{\cdot}$ 0.43 E_1	0.46 E_1 0.33 $E_1^{\cdot}$ 0.16 E_7	0.58 E_7 0.25 E_8	0.44 E_8 0.25 E_7 0.21 E_9	0.67 E_9 0.30 E_8	0.49 $E_3^{\cdot}$ 0.26 E_3 0.23 E_{10}	0.54 E_3 0.40 $E_3^{\cdot}$	0.70 E_{10} 0.20 E_3	0.51 E_4 0.48 $E_4^{\cdot}$	0.51 E_4 0.48 $E_4^{\cdot}$	0.93 E_5	0.94 $E_5^{\cdot}$
	5.29	5.35	5.42	5.65	5.73	5.97	6.23	6.41	6.51	6.81	6.99	7.06
1.97	0.69 E_7 0.26 E_8	0.39 E_8 0.37 E_9 0.21 E_7	0.59 E_9 0.33 E_8	0.53 E_{10} 0.41 E_1	0.97 $E_1^{\cdot}$	0.54 E_1 0.44 E_{10}	0.96 $E_3^{\cdot}$	0.80 E_3 0.16 E_{11}	0.83 E_{11} 0.16 E_3	0.52 E_4 0.47 $E_4^{\cdot}$	0.50 E_4 0.47 $E_4^{\cdot}$	0.93 E_5
	4.99	5.03	5.11	5.30	5.59	5.72	5.87	5.92	6.01	6.19	6.28	6.32
2.07	0.69 E_7 0.28 E_9	0.38 E_9 0.37 E_8 0.22 E_7	0.59 E_8 0.33 E_9	0.98 E_{10}	0.68 E_{11} 0.19 $E_1^{\cdot}$	0.50 E_1 **0.25 E_{13}** 0.21 $E_1^{\cdot}$	**0.36 E_{12}** 0.31 $E_1^{\cdot}$ 0.19 E_{11}	**0.51 E_{12}** 0.28 $E_1^{\cdot}$	**0.63 E_{13}** 0.23 E_1	0.65 E_{14} 0.30 E_{15}	0.38 E_{15} 0.30 E_{16} 0.30 E_{14}	0.64 E_{16} 0.32 E_{15}
	4.69	4.81	4.88	4.94	4.97	5.05	5.44	5.61	5.74	5.89	5.98	6.04
2.17	0.58 E_7 0.31 E_8	0.35 E_{10} 0.26 E_9 0.24 E_8	0.60 E_9 **0.15 E_{12}**	0.53 E_{10} **0.23 E_{12}**	**0.48 E_{12}** 0.34 E_8	**0.97 E_{13}**	0.71 E_{11} 0.28 E_{14}	0.71 E_{14} 0.28 E_{11}	0.97 E_{15}	0.58 E_{16} 0.33 E_{17}	0.44 E_{18} 0.34 E_{16}	0.48 E_{18} 0.44 E_{17}
	4.41	4.61	4.86	4.90	4.95	4.98	5.06	5.20	5.73	5.80	5.89	5.96
2.27	0.65 E_7 0.33 E_8	0.63 E_8 0.31 E_7	0.76 E_9 0.19 E_{10}	0.57 E_{10} **0.24 E_{12}** 0.15 E_9	**0.62 E_{12}** 0.17 E_{10}	**0.56 E_{13}** 0.17 E_{17}	0.48 E_{17} **0.32 E_{13}** 0.19 E_{11}	0.68 E_{11} 0.31 E_{17}	0.96 E_{18}	0.56 E_{14} 0.35 E_{15}	0.42 E_{16} 0.35 E_{14} 0.21 E_{15}	0.49 E_{16} 0.44 E_{15}
	4.22	4.42	4.71	4.85	4.88	4.90	4.94	4.96	5.72	5.74	5.83	5.90
2.37	0.76 E_7 0.23 E_8	0.75 E_8 0.23 E_7	**0.70 E_{12}** 0.26 E_9	**0.49 E_{13}** 0.41 E_{10}	0.41 E_{17} **0.35 E_{13}**	0.67 E_9 **0.27 E_{12}**	0.41 E_{10} 0.34 E_{17}	0.77 E_{18} 0.15 E_{17}	0.64 E_{11} 0.17 E_{14}	0.36 E_{14} 0.33 E_{11} 0.24 E_{15}	0.42 E_{16} 0.38 E_{14} 0.18 E_{15}	0.48 E_{16} 0.43 E_{15}
	3.99	4.21	4.44	4.63	4.89	4.93	4.98	5.00	5.67	5.72	5.78	5.85
2.47	**0.73 E_{12}** **0.27 E_{13}**	**0.72 E_{13}** **0.27 E_{12}**	0.74 E_7 0.26 E_8	0.74 E_8 0.26 E_7	0.72 E_9 0.27 E_{10}	0.54 E_9 0.22 E_{10} 0.21 E_{17}	0.46 E_{17} 0.45 E_{18}	0.50 E_{18} 0.32 E_{17}	0.37 E_{14} 0.30 E_{15} 0.24 E_{11}	0.72 E_{11} 0.16 E_{14}	0.39 E_{14} 0.39 E_{16} 0.20 E_{15}	0.50 E_{16} 0.42 E_{15}
	3.84	4.06	4.24	4.41	4.90	4.94	4.98	5.02	5.62	5.69	5.73	5.80
2.57	**0.75 E_{12}** **0.25 E_{13}**	**0.74 E_{13}** **0.25 E_{12}**	0.68 E_7 0.32 E_{17}	0.68 E_{17} 0.32 E_7	0.74 E_8 0.23 E_{18}	0.55 E_{18} 0.18 E_8 0.18 E_9	0.64 E_9 0.26 E_{10}	0.64 E_{10} 0.15 E_9 0.15E_{18}	0.31 E_{15} 0.30 E_{14} 0.29 E_{11}	0.58 E_{11} 0.30 E_{14}	0.37 E_{16} 0.33 E_{14} 0.21 E_{15}	0.51 E_{16} 0.41 E_{15}
	3.70	3.91	4.05	4.22	4.91	4,95	4.98	5.03	5.57	5.66	5.68	5.75
2.67	**0.70 E_{12}** **0.30 E_{13}**	**0.70 E_{13}** **0.30 E_{12}**	0.61 E_{17} 0.39 E_{18}	0.61 E_{18} 0.39 E_{17}	0.77 E_{14} 0.21 E_{15}	0.59 E_{15} 0.15 E_{14}	0.70 E_{16} 0.23 E_{17}	0.63 E_{17} 0.17 E_{15}	0.44 E_{14} 0.27 E_{15} 0.18 E_{11}	0.55 E_{11} 0.31 E_{14}	0.33 E_{16} 0.26 E_{15} 0.20 E_{11} 0.18 E_{14}	0.51 E_{16} 0.39 E_{15}

As shown in Figure 7 (middle panel), the incremental occupation of the σ-σ*-σ orbital upon N-N distance elongation results in an initially slow but steady decrease in N-N EBO from 2.37 to 1.86 between the equilibrium structure and 1.87 Å, followed by a rapid drop to ca. 0.9 at distances greater than 1.97 Å and finally 0.5 beyond 2.27 Å N-N separation (dark blue trace). These steps coincide with the switch in ground state from the CASSCF states E_1 to the set of E_7, E_8, E_9, E_{10} states and E_{12}, E_{13} states. The Os-N bond order increases concomittantly (light blue trace). The difference in occupation number of N-N(σ/σ*) and Os-N(π/π*) orbitals can be taken as an indicator of their energetic similarity (Fig. 7, lowest panel). The occupation number difference for the σ orbitals shows a stepwise decrease from 1.96 to 0.92 to 0.02, which is mirrored by an increased occupation number difference for the Os-N π* orbitals as the π*-π-π* orbital is depopulated. It is noted that along the scan, the orbital character of specific π-orbitals changes while maintaining the correct symmetry. The top panel in Figure 7 shows changes in representative σ and π orbitals along the N-N dissociation coordinate. The σ-σ-σ orbital shows a more pronounced dent in the red lobe as the N-N distance increases, and the π-π*-π orbitals localize on opposite sides of the monomer (only one shown). Changes in the character of mostly antibonding orbitals are less pronounced. Taken together, these data can be interpreted as a sequential breaking of the N-N σ bond along the N-N dissociation coordinate, in parallel to the gradual occupation of π*-type MOs and their transformation from dimeric to monomeric.

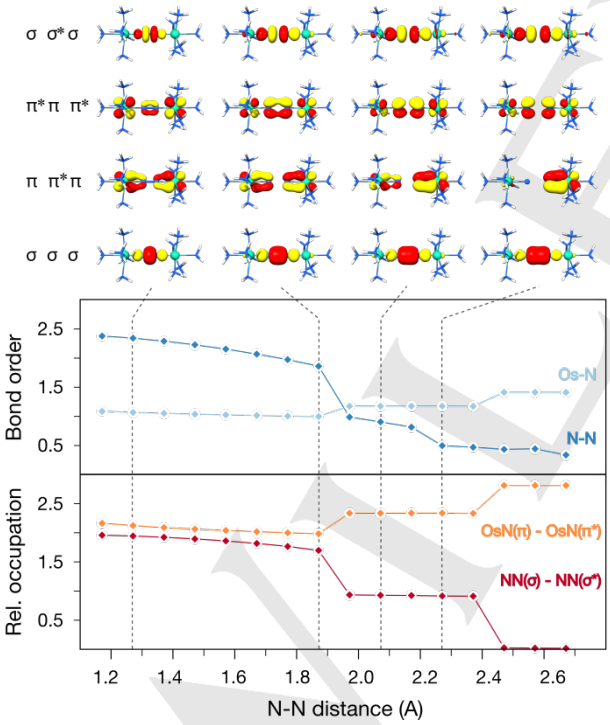

Figure 7. Changes in descriptors of the electronic structure along the N-N dissociation coordinate. Top: represenative orbitals for *d*(N-N) = 1.271 Å, 1.871 Å, 2.071 Å, 2.271 Å; middle: Os-N (light blue) and N-N (dark blue) bond orders; bottom: relative occupation numbers of σ/σ* and π/π* orbitals.

These results and considerations, in combination with basic MO theory, allow us to deduce a comprehensive picture of the required electronic structure changes along the N-N dissociation coordinate (Fig. 8). Increasing the N-N distance leads to a smaller overlap between the N p_z atomic orbital components, thus a weaker splitting of the N-N σ/σ* levels which results in a lowered energy of the σ-σ*-σ MO. As the σ-σ*-σ orbital becomes degenerate with the occupied π*-π-π* level, the MO occupation pattern changes such that the electrons from the former HOMOs, π*-π-π*, move to the σ-σ*-σ MO. This weakens the N-N bond due to the population of an orbital with N-N σ* character, while concomittantly strengthening the Os-N π bond due to the depopulation of an orbital with Os-N π* character. The subsequent degeneracy of the σ-σ*-σ MO with the two orbitals of δ(xy)/δ*(xy) character should have a much smaller effect on the electronic structure since the orbital occupation pattern remains unchanged. At the end of the N_2 cleavage process, once the monomers are fully formed, the former σ-σ*-σ MO is finally equal in energy to the σ-σ-σ orbital (Fig. 8). At this point, similar to the localization of the π MOs, the d(xy) and $d(x^2-y^2)$ orbitals would not form δ/δ* combinations anymore, and the σ MOs would correspond to monomeric $Os(d_{z2})$-$N(p_z)$ orbitals.

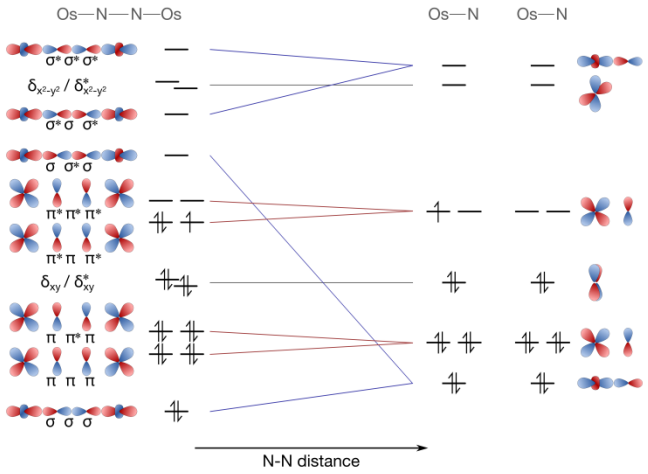

Figure 8. Changes in the MO diagram of **1** upon N-N cleavage. The MO diagrams are not drawn to scale; for better legibility the monomeric non-bonding d(xy) and $d(x^2-y^2)$ orbitals are kept at the same energy as in the dimer.

Conclusions

We have shown that the challenging electronic structure of the valence-deloalized osmium dimer $[Os^{(II,III)}_2(\mu\text{-}N_2)(NH_3)_{10}]^{5+}$ can be described adequately with CASPT2/CASSCF calculations with different types and sizes of active space. The lowest states above the $(\sigma\text{-}\sigma\text{-}\sigma)^2(\pi\text{-}\pi\text{-}\pi)^4(\pi\text{-}\pi^*\text{-}\pi)^4(\delta_{xy})^2(\delta^*_{xy})^2(\pi^*\text{-}\pi\text{-}\pi^*)^3(\pi^*\text{-}\pi^*\text{-}\pi^*)^0(\sigma\text{-}\sigma^*\text{-}\sigma)^0(\sigma^*\text{-}\sigma\text{-}\sigma^*)^0(\delta_{x2\text{-}y2})^0(\delta^*_{x2\text{-}y2})^0(\sigma^*\text{-}\sigma^*\text{-}\sigma^*)^0$ degenerate doublet ground state are best described as $^2[((\delta(xy)/\delta(xy)^*)^3(\pi^*\text{-}\pi\text{-}\pi^*)^4) + (\delta(xy)/\delta(xy)^*)^3(\pi^*\text{-}\pi\text{-}\pi^*)^3(\pi^*\text{-}\pi^*\text{-}\pi^*)^1]$ and $^2[(\pi\text{-}\pi^*\text{-}\pi)^1(\pi^*\text{-}\pi\text{-}\pi^*)^4 + (\pi^*\text{-}\pi\text{-}\pi^*)^2(\pi^*\text{-}\pi^*\text{-}\pi^*)^1]$, followed by a dense set of ca. 30 doublet and ca. 18 quartet states several eV above the ground state. On the basis of this electronic structure description, it was shown that the low-energy features in the UV-vis absorption spectrum are dominated by excitations of the type $\delta(xy)/\delta(xy)^* \rightarrow \pi^*\text{-}\pi\text{-}\pi^*$ and π-

π*-π→π*-π-π*, in excellent agreement with the experimental spectrum and its previous assignment.

A scan along the N-N dissociation coordinate revealed that dinitrogen breaks in two steps: the σ-σ*-σ orbital is lowered in energy and becomes singly occupied between ca. 1.97-2.37 Å, while above 2.47 Å it is low enough in energy to be doubly occupied. The degrees of freedom not considered in this scan, namely the relaxation of Os-N distances and Os-NH_3 distances as well as possible rotations about the N-N axis, are expected to result in only minor perturbations of the general picture obtained above. Further insight into all photophysical and photochemical processes involved in dinitrogen photocleavage with **1** could be obtained with *ab initio* excited state dynamics,[30] but the underlying required on-the-fly electronic structure calculations are currently computationally too demanding to follow this route.

Based on the results obtained here, we can presently only speculate about the nature of the excitation that ultimately breaks the dinitrogen bond. Two basic scenarios can be envisaged: (i) an excitation that leads to a geometric distortion of the Os-N-N-Os core in the excited state which lowers the energy of an MO with N-N σ* character, i.e. σ-σ*-σ, such that it can become doubly occupied, and (ii) an excitation that directly leads to a significant (single or double) occupation of the σ-σ*-σ orbital with subsequent separation of the fragments that would then already have the orbital occupation pattern of the monomers. Scenario (ii) with a double excitation of the type π*-π-π*→σ-σ*-σ would certainly be the most straightforward solution, and given the significant number of double excitations found at higher energies for the (13,10) and (15,10) active spaces, this is not far-fetched. This study showed however that it will be very difficult, if not impossible, to identify the energetic position of states with significant contributions of $(\sigma\text{-}\sigma^*\text{-}\sigma)^1/(\sigma\text{-}\sigma^*\text{-}\sigma)^2$-occupied configurations at the ground state geometry with CASSCF calculations due to the high density of electronic states below the excitation energies that induce N_2 photocleavage in **1**.

The idea of using electronic excitations to populate a N-N antibonding orbital to induce N_2 splitting has been discussed before. In a thought experiment by Fischler and von Gustorf, they noted that an excitation from a π- to a σ*-orbital in coordinated N_2 would weaken the N-N bond in a twofold way but not redistribute electron density at the metal, while a MLCT transition into a π*-orbital would increase the nitrogen basicity and thus facilitate protonation.[31] The previous computational study by Reiher et al. investigated a HOMO-LUMO transition populating a π*-orbital in the S_1 state of Fe and Ru complexes, which would subsequently relax to a bent M-N-N-M structure that can be protonated more easily.[13]

For the osmium dimer studied here, correlating the MO diagrams of the osmium dimer and the two resulting osmium-nitrido monomers, shows that the orbital of central importance to the N_2 photocleavage process is the σ-σ*-σ orbital. We therefore conclude from this study that the key step in dinitrogen cleavage is a geometric distortion that makes the unoccupied MO with dominant N-N σ* character equal in energy to the HOMO, whichever character this orbital may have. We believe that this is a general conclusion that will be equally valid for thermal dinitrogen cleavage processes with linear M-N-N-M cores. Importantly, this also implies that to lower the activation barrier for N_2 cleavage, the energetic separation between the σ-σ*-σ MO and the HOMO ought to be lowered. It remains to be explored in future theoretical and experimental studies how to design the geometric and electronic structure of N_2-fixation catalysts to achieve this. Obvious starting points are the metal coordination geometry, metal oxidation states, and electronic properties of ligands, especially those *trans* to the μ-N_2 ligand. For instance, if the HOMO were an orbital of δ(xy)/δ*(xy) character, the transfer of electrons upon elongation of the N-N bond would be less effective than in the present case, as it would only weaken the N-N bond, but not strengthen the Os-N bond at the same time.

Computational Details

All geometry optimizations were carried out with the ORCA program package,[32] using the BP86 density functional[33] including the resolution of the identity (RI) approximation[34] and zeroth-order scalar relativistic (ZORA) effects retaining one-center terms[35] together with ZORA-recontraceted versions of Ahlrich's def2-TZVP basis set and a decontracted auxiliary def2-TZVP/J basis.[36] Dispersion corrections with Becke-Johnson damping (D3BJ) according to Grimme were used.[37] The integration grid and integration accuracy were both increased to 7 in ORCA nomenclature. Tight SCF convergence criteria were chosen, and the one-center approximation was employed. Inclusion of the COSMO solvation model[38] for water changed the geometry from eclipsed from the optimization in vacuum to eclipsed.

All CASSCF and CASPT2 calculations were carried out with MOLCAS using default settings unless stated otherwise.[39] The calculations employed the Cholesky decomposition with auxiliary basis sets generated on-the-fly and atomic mean-field integrals for spin-orbit coupling,[40] as well as the Douglas–Kroll–Hess (DKH) to second order as the relativistic operator.[41] The active space size, basis set and number of roots is given in the main text as appropriate. Generally, the ANO-RCC-MB basis set was used for H atoms, and either the ANO-RCC-MB or ANO-RCC-VDZP on Os and N atoms.[42] A comparison of basis set effects is given in the SI, Table SY. In CASPT2 calculations, no level shift but an imaginary shift of 0.1 was employed. Internally consistent reference weights above 0.5 were obtained (average: 0.54, std. dev. < 0.01).

RASSI calculations included spin-orbit coupling effects[43] and were used to predict relative energies and oscillator strengths for the UV-vis absorption spectra. The energies and intensities derived from the RASSI program were convoluted with Gaussian lineshapes with a FWHM of 0.1 eV and normalized such that the highest-intensity transition matches the most intense feature in the experimental spectrum.

Bond orders were calculated from the orbital occupation numbers as detailed in the main text. For Figure 7, the N-N bond orders at each point of the scan were calculated with the σ-σ-σ, π-π-π, π*-π-π* and σ*-σ-σ* orbitals as N-N bonding and the π-π*-π, π*-π*-π*, σ-σ*-σ and σ*-σ*-σ* as N-N antibonding, while for the Os-N bond orders the π-π-π and π-π*-π orbitals were taken as bonding and the π*-π-π* and π*-π*-π* as antibonding. The differences in occupation numbers were calculated as η(σ*-σ-σ*)–η(σ*-σ*-σ*) orbitals, and $0.5[\eta(\pi\text{-}\pi\text{-}\pi + \pi\text{-}\pi^*\text{-}\pi)\text{-}\eta(\pi^*\text{-}\pi\text{-}\pi^* + \pi^*\text{-}\pi^*\text{-}\pi^*)]$.

Acknowledgements

This research was funded by a H2020 Marie-S.-Curie Individual Fellowship of the European Commission, call H2020-MSCA-IF-2015, proposal number 703860, title: Solar Dinitrogen Activation, acronym: SolarAct. A Prize Fellowship from the University of Bath is gratefully acknowledged (VK). The COST action CM1305 "Explicit Control Over Spin-states in Technology and Biochemistry (ECOSTBio)" is gratefully acknowledged for first introducing the authors as well as network support.

Keywords: Nitrogen fixation • ab initio calculations • transition metals • osmium • mixed-valent compounds •

References

[1] M. J. Bezdek and P. J. Chirik, *Angewandte Chemie International Edition* **2016**, *55*, 7892-7896.

[2] a) T. Kandemir, M. E. Schuster, A. Senyshyn, M. Behrens and R. Schlögl, *Angewandte Chemie International Edition* **2013**, *52*, 12723-12726; b) N. Cherkasov, A. O. Ibhadon and P. Fitzpatrick, *Chemical Engineering and Processing: Process Intensification* **2015**, *90*, 24-33.

[3] R. Schlögl, *Angewandte Chemie International Edition* **2003**, *42*, 2004-2008.

[4] V. Krewald, M. Retegan and D. A. Pantazis, *Top Curr Chem* **2016**, *371*, 23-48.

[5] a) H. Dau and I. Zaharieva, *Accounts of Chemical Research* **2009**, *42*, 1861-1870; b) D. G. Nocera, *Accounts of Chemical Research* **2012**, *45*, 767-776; c) K. J. Young, L. A. Martini, R. L. Milot, R. C. Snoeberger Iii, V. S. Batista, C. A. Schmuttenmaer, R. H. Crabtree and G. W. Brudvig, *Coordination Chemistry Reviews* **2012**, *256*, 2503-2520.

[6] a) G. J. Christian, R. N. L. Terrett, R. Stranger, G. Cavigliasso and B. F. Yates, *Chemistry – A European Journal* **2009**, *15*, 11373-11383; b) J. L. Crossland and D. R. Tyler, *Coordination Chemistry Reviews* **2010**, *254*, 1883-1894; c) B. M. Hoffman, D. Lukoyanov, Z.-Y. Yang, D. R. Dean and L. C. Seefeldt, *Chemical Reviews* **2014**, *114*, 4041-4062; d) F. Barrière in *Model Complexes of the Active Site of Nitrogenases: Recent Advances*, Wiley-VCH Verlag GmbH & Co. KGaA, **2014**, pp. 225-248; e) Y. Hu and M. W. Ribbe, *Angewandte Chemie International Edition* **2016**, *55*, 8216-8226; f) M. D. Walter in *Chapter Five - Recent Advances in Transition Metal-Catalyzed Dinitrogen Activation*, *Vol. Volume 65* (Ed. J. P. Pedro), Academic Press, **2016**, pp. 261-377; g) I. Čorić and P. L. Holland, *Journal of the American Chemical Society* **2016**, *138*, 7200-7211; h) F. S. Schendzielorz, M. Finger, C. Volkmann, C. Würtele and S. Schneider, *Angewandte Chemie International Edition* **2016**, *55*, 11417-11420; i) N. S. Sickerman, K. Tanifuji, Y. Hu and M. W. Ribbe, *Chemistry* **2017**, *23*, 12425-12432; j) B. Wang, G. Luo, M. Nishiura, S. Hu, T. Shima, Y. Luo and Z. Hou, *Journal of the American Chemical Society* **2017**, *139*, 1818-1821; k) I. Klopsch, E. Y. Yuzik-Klimova and S. Schneider, **2017**, *60*, 71-112.

[7] a) C. E. Laplaza and C. C. Cummins, *Science* **1995**, *268*, 861-863; b) R. R. Schrock, *Accounts of Chemical Research* **2005**, *38*, 955-962; c) K. Arashiba, E. Kinoshita, S. Kuriyama, A. Eizawa, K. Nakajima, H. Tanaka, K. Yoshizawa and Y. Nishibayashi, *Journal of the American Chemical Society* **2015**; d) J. Rittle and J. C. Peters, *Journal of the American Chemical Society* **2016**, *138*, 4243-4248; e) Y. Roux, C. Duboc and M. Gennari, *Chemphyschem* **2017**, *18*, 2606-2617; f) G. A. Silantyev, M. Förster, B. Schluschaß, J. Abbenseth, C. Würtele, C. Volkmann, M. C. Holthausen and S. Schneider, *Angewandte Chemie International Edition* **2017**, *56*, 5872-5876.

[8] a) M. P. Shaver and M. D. Fryzuk, *Advanced Synthesis & Catalysis* **2003**, *345*, 1061-1076; b) K. C. MacLeod and P. L. Holland, *Nat Chem* **2013**, *5*, 559-565.

[9] a) J. Du Bois, C. S. Tomooka, J. Hong and E. M. Carreira, *Accounts of Chemical Research* **1997**, *30*, 364-372; b) J. V. Ruppel, J. E. Jones, C. A. Huff, R. M. Kamble, Y. Chen and X. P. Zhang, *Organic Letters* **2008**, *10*, 1995-1998; c) J. M. Smith in *Reactive Transition Metal Nitride Complexes*, John Wiley & Sons, Inc., **2014**, pp. 417-470; d) W.-L. Man, W. W. Y. Lam and T.-C. Lau, *Accounts of Chemical Research* **2014**, *47*, 427-439; e) A. J. Keane, W. S. Farrell, B. L. Yonke, P. Y. Zavalij and L. R. Sita, *Angewandte Chemie International Edition* **2015**, *54*, 10220-10224; f) R. M. Clarke and T. Storr, *Journal of the American Chemical Society* **2016**, *138*, 15299-15302; g) I. Klopsch, M. Kinauer, M. Finger, C. Würtele and S. Schneider, *Angewandte Chemie International Edition* **2016**, n/a-n/a; h) J. Li, J. Yin, C. Yu, W. Zhang and Z. Xi, *Acta Chimica Sinica* **2017**, *75*; i) M. Falcone, L. Chatelain, R. Scopelliti, I. Živković and M. Mazzanti, *Nature* **2017**, *547*, 332-335; j) Y. Nakanishi, Y. Ishida and H. Kawaguchi, *Angewandte Chemie International Edition* **2017**, *56*, 9193-9197.

[10] a) C. Rebreyend and B. de Bruin, *Angewandte Chemie International Edition* **2015**, *54*, 42-44; b) A. J. Medford and M. C. Hatzell, *ACS Catalysis* **2017**, *7*, 2624-2643.

[11] a) O. Rusina, A. Eremenko, G. Frank, H. P. Strunk and H. Kisch, *Angewandte Chemie International Edition* **2001**, *40*, 3993-3995; b) T. Oshikiri, K. Ueno and H. Misawa, *Angewandte Chemie* **2016**, *55*, 3942-3946; c) J. M. P. Martirez and E. A. Carter, *Journal of the American Chemical Society* **2017**, *139*, 4390-4398.

[12] a) E. Solari, C. Da Silva, B. Iacono, J. Hesschenbrouck, C. Rizzoli, R. Scopelliti and C. Floriani, *Angewandte Chemie International Edition* **2001**, *40*, 3907-3909; b) H. Kunkely and A. Vogler, *Angewandte Chemie International Edition* **2010**, *49*, 1591-1593; c) A. S. Huss, J. J. Curley, C. C. Cummins and D. A. Blank, *The Journal of Physical Chemistry B* **2013**, *117*, 1429-1436; d) T. Miyazaki, H. Tanaka, Y. Tanabe, M. Yuki, K. Nakajima, K. Yoshizawa and Y. Nishibayashi, *Angewandte Chemie International Edition* **2014**, *53*, 11488-11492; e) T. M. Buscagan, P. H. Oyala and J. C. Peters, *Angewandte Chemie International Edition* **2017**, *56*, 6921-6926.

[13] M. Reiher, B. Kirchner, J. Hutter, D. Sellmann and B. A. Hess, *Chemistry – A European Journal* **2004**, *10*, 4443-4453.

[14] J. J. Curley, T. R. Cook, S. Y. Reece, P. Müller and C. C. Cummins, *Journal of the American Chemical Society* **2008**, *130*, 9394-9405.

[15] B. Kirchner, M. Reiher, A. Hille, J. Hutter and B. A. Hess, *Chemistry* **2005**, *11*, 574-583.

[16] D. E. Richardson, J. P. Sen, J. D. Buhr and H. Taube, *Inorganic Chemistry* **1982**, *21*, 3136-3140.

[17] P. A. Lay, R. H. Magnuson, H. Taube, J. Ferguson and E. R. Krausz, *Journal of the American Chemical Society* **1985**, *107*, 2551-2552.

[18] a) D. E. Richardson and H. Taube, *Coordination Chemistry Reviews* **1984**, *60*, 107-129; b) D. Yokogawa, H. Sato, Y. Nakao and S. Sakaki, *Inorganic Chemistry* **2007**, *46*, 1966-1974; c) J. J. Concepcion, D. M. Dattelbaum, T. J. Meyer and R. C. Rocha, *Philosophical Transactions of the Royal Society A: Mathematical, Physical and Engineering Sciences* **2008**, *366*, 163-175.

[19] C. Creutz and H. Taube, *Journal of the American Chemical Society* **1969**, *91*, 3988-3989.

[20] a) M. B. Robin and P. Day in *Mixed Valence Chemistry-A Survey and Classification*, *Vol. Volume 10* Eds.: H. J. Emeléus and A. G. Sharpe), Academic Press, **1968**, pp. 247-422; b) M. Parthey and M. Kaupp, *Chemical Society Reviews* **2014**, *43*, 5067-5088.

[21] R. H. Magnuson and H. Taube, *Journal of the American Chemical Society* **1972**, *94*, 7213-&.

[22] C.-M. Che, H.-W. Lam, W.-F. Tong, T.-F. Lai and T.-C. Lau, *Journal of the Chemical Society, Chemical Communications* **1989**, 1883-1884.

[23] P. L. Holland, *Dalton Transactions* **2010**, *39*, 5415-5425.

[24] K. D. Demadis, T. J. Meyer and P. S. White, *Inorganic Chemistry* **1997**, *36*, 5678-5679.

[25] P. A. Lay and W. D. Harman in *Recent Advances in Osmium Chemistry*, *Vol. Volume 37* (Ed. A. G. Sykes), Academic Press, **1991**, pp. 219-379.

[26] L. Dubicki, J. Ferguson, E. R. Krausz, P. A. Lay, M. Maeder, R. H. Magnuson and H. Taube, *Journal of the American Chemical Society* **1985**, *107*, 2167-2171.

[27] a) M. Brynda, L. Gagliardi, P. O. Widmark, P. P. Power and B. O. Roos, *Angew Chem Int Ed Engl* **2006**, *45*, 3804-3807; b) B. O. Roos, A. C. Borin and L. Gagliardi, *Angew Chem Int Ed Engl* **2007**, *46*, 1469-1472; c) G. Li Manni, A. L. Dzubak, A. Mulla, D. W. Brogden, J. F. Berry and L. Gagliardi, *Chemistry* **2012**, *18*, 1737-1749.

[28] a) M. Srnec, J. Chalupsky, M. Fojta, L. Zendlova, L. Havran, M. Hocek, M. Kyvala and L. Rulisek, *J Am Chem Soc* **2008**, *130*, 10947-10954; b) J. P. Malrieu, R. Caballol, C. J. Calzado, C. de Graaf and N. Guihéry, *Chemical Reviews* **2014**, *114*, 429-492.

[29] a) K. M. Neyman, V. A. Nasluzov, J. Hahn, C. R. Landis and N. Rösch, *Organometallics* **1997**, *16*, 995-1000; b) D. C. Graham, G. J. O. Beran, M. Head-Gordon, G. Christian, R. Stranger and B. F. Yates, *The Journal of Physical Chemistry A* **2005**, *109*, 6762-6772; c) I. Klopsch, M. Finger, C. Würtele, B. Milde, D. B. Werz and S. Schneider, *Journal of the American Chemical Society* **2014**, *136*, 6881-6883.

[30] a) D. Marx and J. Hutter, **2009**; b) M. Richter, P. Marquetand, J. González-Vázquez, I. Sola and L. González, *Journal of Chemical Theory and Computation* **2011**, *7*, 1253-1258; c) S. Mai, P. Marquetand and L. González, *International Journal of Quantum Chemistry* **2015**, *115*, 1215-1231.

[31] I. Fischler and E. K. von Gustorf, *Naturwissenschaften* **1975**, *62*, 63-70.

[32] F. Neese, *Wiley Interdisciplinary Reviews: Computational Molecular Science* **2012**, *2*, 73-78.

[33] a) J. P. Perdew, *Physical Review B* **1986**, *33*, 8822-8824; b) A. D. Becke, *Physical Review A* **1988**, *38*, 3098-3100.

[34] a) B. I. Dunlap, J. W. D. Connolly and J. R. Sabin, *The Journal of Chemical Physics* **1979**, *71*, 3396-3402; b) M. Feyereisen, G. Fitzgerald and A. Komornicki, *Chemical Physics Letters* **1993**, *208*, 359-363.

[35] a) E. van Lenthe, E. J. Baerends and J. G. Snijders, *Journal of Chemical Physics* **1994**, *101*, 9783-9792; b) E. van Lenthe, J. G. Snijders and E. J. Baerends, *Journal of Chemical Physics* **1996**, *105*, 6505-6516.

[36] a) F. Weigend and R. Ahlrichs, *Physical Chemistry Chemical Physics* **2005**, *7*, 3297-3305; b) F. Weigend, *Physical Chemistry Chemical Physics* **2006**, *8*, 1057-1065; c) D. A. Pantazis, X. Y. Chen, C. R. Landis and F. Neese, *Journal of Chemical Theory and Computation* **2008**, *4*, 908-919; d) D. A. Pantazis and F. Neese, *Journal of Chemical Theory and Computation* **2009**, *5*, 2229-2238.

[37] a) S. Grimme, J. Antony, S. Ehrlich and H. Krieg, *Journal of Chemical Physics* **2010**, *132*, 154104-154119; b) S. Grimme, S. Ehrlich and L. Goerigk, *Journal of Computational Chemistry* **2011**, *32*, 1456-1465.

[38] A. Klamt and D. Schüürman, *Journal of the Chemical Society, Perkin Transactions 2: Physical Organic Chemistry* **1993**, 799-805.

[39] a) F. Aquilante, J. Autschbach, R. K. Carlson, L. F. Chibotaru, M. G. Delcey, L. De Vico, I. Fdez Galvan, N. Ferre, L. M. Frutos, L. Gagliardi, M. Garavelli, A. Giussani, C. E. Hoyer, G. Li Manni, H. Lischka, D. Ma, P. A. Malmqvist, T. Muller, A. Nenov, M. Olivucci, T. B. Pedersen, D. Peng, F. Plasser, B. Pritchard, M. Reiher, I. Rivalta, I. Schapiro, J. Segarra-Marti, M. Stenrup, D. G. Truhlar, L. Ungur, A. Valentini, S. Vancoillie, V. Veryazov, V. P. Vysotskiy, O. Weingart, F. Zapata and R. Lindh, *J Comput Chem* **2016**, *37*, 506-541; b) H. J. Werner and W. Meyer, *The Journal of Chemical Physics* **1980**, *73*, 2342-2356; c) B. O. Roos, P. R. Taylor and P. E. M. Siegbahn, *Chemical Physics* **1980**, *48*, 157-173; d) K. Andersson, P. A. Malmqvist, B. O. Roos, A. J. Sadlej and K. Wolinski, *The Journal of Physical Chemistry* **1990**, *94*, 5483-5488.

[40] a) N. H. F. Beebe and J. Linderberg, *International Journal of Quantum Chemistry* **1977**, *12*, 683-705; b) H. Koch, A. Sánchez de Merás and T. B. Pedersen, *The Journal of Chemical Physics* **2003**, *118*, 9481-9484; c) F. Aquilante, P. A. Malmqvist, T. B. Pedersen, A. Ghosh and B. O. Roos, *J Chem Theory Comput* **2008**, *4*, 694-702; d) F. Aquilante, T. B. Pedersen, R. Lindh, B. O. Roos, A. Sanchez de Meras and H. Koch, *J Chem Phys* **2008**, *129*, 024113; e) T. B. Pedersen, F. Aquilante and R. Lindh, *Theoretical Chemistry Accounts* **2009**, *124*, 1-10.

[41] a) B. A. Hess, *Physical Review A* **1985**, *32*, 756-763; b) B. A. Hess, *Physical Review A* **1986**, *33*, 3742-3748; c) G. Jansen and B. A. Hess, *Physical Review A* **1989**, *39*, 6016-6017.

[42] B. O. Roos, R. Lindh, P.-Å. Malmqvist, V. Veryazov and P.-O. Widmark, *Journal of Physical Chemistry A* **2005**, *109*, 6575-6579.

[43] P.-Å. Malmqvist, B. O. Roos and B. Schimmelpfennig, *Chemical Physics Letters* **2002**, *357*, 230-240.